ADVANCED FUNCTIONAL MATERIALS
www.afm-journal.de

Piezoelectric Nylon-11 Fibers for Electronic Textiles, Energy Harvesting and Sensing

*Saleem Anwar, Morteza Hassanpour Amiri, Shuai Jiang, Mohammad Mahdi Abolhasani, Paulo R. F. Rocha, and Kamal Asadi**

Electronic textiles and functional fabrics are among the key constituents envisioned for wearable electronics applications. For e-textiles, the challenge is to process materials of desired electronic properties such as piezoelectricity into fibers to be integrated as wefts or wraps in the fabrics. Nylons, first introduced in the 1940s for stockings, are among the most widely used synthetic fibers in textiles. However, realization of nylon-based e-textiles has remained elusive due to the difficulty of achieving the piezoelectric phase in the nylon fibers. Here, piezoelectric nylon-11 fibers are demonstrated and it is shown that the resulting fibers are viable for applications in energy harvesting from low frequency mechanical vibrations and in motion sensors. A simulation study is presented that elucidates on the sensitivity of the nylon-11 fibers toward external mechanical stimuli. Moreover, a strategy is proposed and validated to significantly boost the electrical performance of the fibers. Since a large fraction of the textile industry is based on nylon fibers, the demonstration of piezoelectric nylon fibers will be a major step toward realization of electronic textiles for applications in apparels, health monitoring, sportswear, and portable energy generation.

1. Introduction

Electronic textiles (or e-textiles), a key technology enabler for the emerging artificial skins and smart garments, seamlessly integrate electronic elements such as pressure sensors, actuators, and microcontrollers in a fabric.[1–3] Textiles that generate electricity from the environment have been suggested as a promising replacement to batteries, to supply the power that is needed for driving the electronics used in the same fabric.[1,2,4] Piezoelectric polymers are ideal for energy harvesting in e-textiles because of the omnipresence of mechanical vibrations or deformations, which can be converted into electricity.[5] Furthermore, such polymers have relatively large piezoelectric voltage coefficients, which renders them as the ideal materials for pressure sensing[6–9] ideally suited for application in artificial skins. Regardless of the envisioned application, the first step toward a piezoelectric fabric is to realize fibers that are piezoelectric.

Nylons (or polyamides) fibers, introduced in the 1940s' for the first time in stockings, are one of the most successful synthetic fibers with a well-established textile industry.[10,11] Within the family, odd-nylons constitute the natural choice for realization of e-textiles if crystalized in their piezoelectric phase. For instance, nylon-11, the well-studied odd-nylons, has various crystalline phases, namely α, α', γ, and δ' of which only the δ'-phase shows strong piezoelectric activity. The triclinic α-phase (similarly α'-phase) is strongly hydrogen bonded.[12,13] Polycrystalline films of α- or α'-phase nylon-11 do not show piezoelectricity due to random polarity of the crystalline domains, which cannot be aligned by electric poling because the strong inter-chain hydrogen bonding necessitates application of an electric field larger than the breakdown field. The γ-phase is

Dr. S. Anwar, M. Hassanpour Amiri, S. Jiang, Dr. M. M. Abolhasani, Prof. K. Asadi
Max-Planck Institute for Polymer Research
Ackermannweg 10, Mainz, Germany
E-mail: asadi@mpip-mainz.mpg.de

Dr. S. Anwar
School of Chemical & Materials Engineering
National University of Sciences & Technology
Sector H-12, Islamabad, Pakistan

The ORCID identification number(s) for the author(s) of this article can be found under https://doi.org/10.1002/adfm.202004326.

DOI: 10.1002/adfm.202004326

Dr. P. R. F. Rocha
Centre for Biosensors, Bioelectronics and Biodevices (C3Bio)
Department of Electronic and Electrical Engineering
University of Bath
Claverton Down, Bath BA2 7AY, UK

Dr. P. R. F. Rocha
Centre for Functional Ecology (CFE)
Department of Life Sciences
University of Coimbra
Coimbra 3000-456, Portugal

Prof. K. Asadi
Department of Physics
University of Bath
Claverton Down, Bath BA2 7AY, UK
E-mail: ka787@bath.ac.uk

only slightly polar, shows weak switchable dipole and therefore has weak piezoelectric activity.[12] In contrast, the δ'-phase[12,14–22] has a highly polar smectic pseudohexagonal chain arrangement with poorly organized hydrogen bonds between the chains. The switchability of the dipoles upon application of an external electric field allows for poling of the δ'-phase nylon-11 and to achieve a strong piezoelectric activity.[23,24]

E-textiles based on piezoelectric nylon-11 have never been realized because of the difficulties in achieving the piezoelectric δ'-phase in nylon-11 fibers. The conventional fiber production methods, melt extrusion and melt spinning, produce non-piezoelectric polycrystalline α-phase nylon fibers with a thickness of tens of micrometer.[10,13] Solution casting of nylon-11 from trifluoroacetic acid (TFA) or treating the α-phase in sodium hydroxide salt solution[25] produces the Υ'-phase.[12] Recently, a template wetting technique has been employed to produce nylon-11 nanowires for energy harvesting applications.[26] The nanowires typically exhibit a mixture of α- and Υ'-phases instead of the desired piezoelectric δ'-phase.[27] A summary of the very limited literature on piezoelectric purely nylon fibers is given in Table S1, Supporting Information. Clearly, only the weakly polar Υ'-phase nylon has been demonstrated so far, which concomitantly yields low energy harvesting performance with nearly 30 nW cm^{-2}. Fabricating continuous and mechanically robust electrospun fibers from m-cresol, formic acid, and trifluoroacetic acid (typical solvents used in processing of nylon) is challenging because the resulting fibers are non-piezoelectric α- or Υ'-phase. Therefore, it is not trivial to achieve the piezoelectric δ'-phase. In this regards, fabrication of δ'-phase nylon fibers with strong piezoelectric response would be a major breakthrough that will pave the way toward realization of e-textiles.

For nylon-11 melts, the cooling rate determines the crystalline structure at room temperature. It has been demonstrated that a very fast cooling of the melt leads to the piezoelectric δ'-phase, whereas a slow cooling favors the formation of the non-piezoelectric phases.[28] It therefore can be speculated that the same δ'-phase can be achieved for fibers processed from solution provided that the solvent is rapidly depleted from the fiber. To that end, low boiling point solvents with high vapor pressure such as TFA are ideal. However, the problem is that TFA molecules may remain inside nylon, even after long exposure to high vacuum (>10^{-3} mbar) due to the formation of strong hydrogen bond between the TFA molecules and the amide moieties on the nylon-11 chains. As a result, fast quench of the solvent cannot be realized and the nylon-11 fibers crystalize in a non-piezoelectric crystalline form, Υ'-phase, rendering the nanofibers impractical for the envisioned applications.

Here, we demonstrate δ'-phase piezoelectric nylon-11 fibers, for the first time to the best of our knowledge, by electrospinning from a carefully designed nylon-11 solution. We propose addition of acetone to nylon solution to facilitate fast depletion of solvent because acetone forms a very strong hydrogen bond with bonding energy of nearly –10 kcal mol^{-1} with TFA.[29] Because of the much stronger affinity of the TFA molecules to form hydrogen bond with acetone than with the amide moieties on nylon chains, upon evaporation the acetone molecules will carry the TFA molecules out of the polymer. Fast evaporation conditions, which imitates fast quenching from the melt, yields the piezoelectric phase in nylon-11 fiber.

The electrospun nylon-11 fibers are suitable for energy harvesting or for sensing applications because the fibers are self-poled and produce voltage upon mechanical vibration or deformation. Through process optimization, it is shown that nylon-11 nonwoven fabric can efficiently harvest the energy of mechanical vibrations and deliver areal power densities as high as 3.1 μW cm^{-2}, two orders of magnitude larger than those based on Υ'-phase nylon fibers. The nylon-11 nanofiber mat mounted on hand can also detect slight motions of the fingers and can therefore be applied as movement sensor. A finite element (FE) simulation study is presented that elucidates the role of crystalline phases and the fiber diameter on the piezoelectric activity. Through FE-simulations, it is substantiated that realization of nylon-11 porous fibers, is a viable strategy to significantly boost the electrical performance of the fibers. The demonstration of piezoelectric nylon fibers with an outlined strategy to enhance the piezoelectric response will be a major step toward for realization of smart and wearable electronic textiles for applications such as in health monitoring, sportswear and portable energy generation.

2. Results and Discussion

2.1. Solvent System

To effectively remove all the TFA molecules from the polymer, mixtures near 1:1 TFA:acetone mole% are needed. Three different TFA:acetone mixtures with 60:40, 50:50, and 40:60 mol% are prepared. The mixture with TFA:acetone 60:40 mol% quickly dissolves nylon-11 at room temperature. The 40:60 mol% TFA:acetone composition however does not dissolve nylon-11, which we attribute to the deshielding of the proton due to an excessive amount of acetone. The 50:50 mixture also dissolves nylon-11. However since the 50:50 mixture is at the border of solubility, we focus only on solvent composition 60:40 mol% TFA:acetone. The boiling point and vapor pressure of the solvent mixture 60:40 mol% TFA:acetone amount to 110 ± 2 °C and 2.5 ± 0.5 kPa. Figure S1, Supporting Information shows 1H NMR spectra for pure TFA and TFA:acetone (60:40 mol%). The proton peak for TFA occurs at 12.47 parts per million (ppm). For the TFA:acetone (60:40 mol%), the proton peak shifts linearly to a higher value of 14.00 ppm. In sharp contrast, proton shift in nylon-11 solution in TFA amount to only 12.58 ppm. The shift in the proton peak position, clearly indicates formation of stronger hydrogen bonds between TFA and acetone.

To confirm the effectiveness of adding acetone in removing TFA from nylon-11, two nylon-11 films are prepared by spin-coating from 5 wt% solution in TFA only and in mixture of TFA:acetone (60:40 mol%). Vacuum quenching technique is used to deplete the solvent.[22] As can be seen from Figure S2, Supporting Information, a huge dielectric loss is observed particularly at low frequencies for the nylon-11 film processed from TFA, which is due to the presence of TFA anions inside the film. In sharp contrast, nylon thin-films processed from TFA:acetone (60:40 mol%) exhibit low dielectric loss due to lack or substantially reduced number of ions. Therefore, addition of acetone is an effective way to substantially remove TFA ions from nylon-11 upon solution processing. For the rest of this work TFA:acetone (60:40 mol%) is used as solvent unless it is explicitly mentioned otherwise.

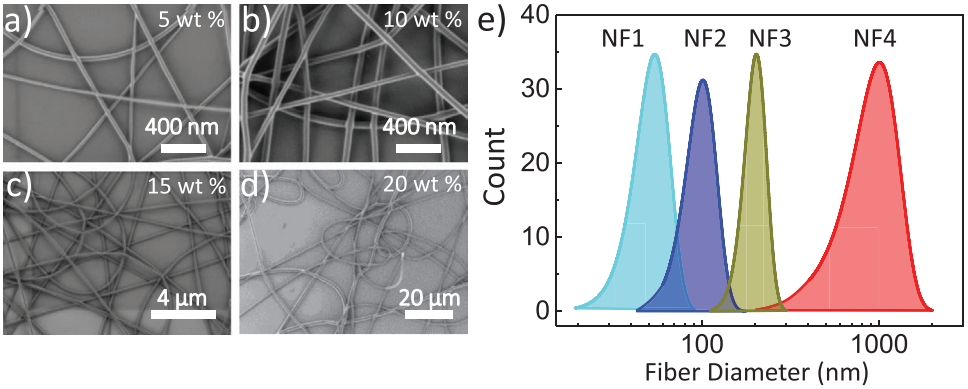

Figure 1. a–d) Representative SEM image of nanofibers NF1 to NF4, showing bead-free electrospun nanofibers. e) Distribution of fiber diameter for NF1, NF2, NF3, and NF4 fibers obtained by measuring of more than 100 fibers from different SEM images.

2.2. Electrospinning Optimization

The schematic of electrospinning setup is shown in Figure S3, Supporting Information. Various parameters are varied to find the optimized process window in order to achieve bead-free nanofibers that are composed of δ' piezoelectric phase. As starting point, nylon-11 fibers are electrospun from 10 wt% solution at 20 kV at a rate of 1 mL h^{-1}. The resulting fibers, Figure S4, Supporting Information, show formation of beads. Subsequently a series of experiments are performed through which the electrospinning parameters are varied systematically. After the optimization process, details are given in Figures S5–S7, Supporting Information, bead-free fibers are obtained. Following the optimization process, the solution concentration and the feed rates are tuned to produce fibers with four different diameters named hereafter NF1 for the thinnest nanofiber to NF4 for the thickest one. A typical scanning electron microscope (SEM) images of randomly aligned bead-free nanofibers with different diameters are given in **Figure 1**a–d. A summary of the resulting fiber diameters for NF1 to NF4 is given in Figure 1e. The diameter of the nylon-11 nanofibers can be accurately tuned through solution concentration and feed rate from 55 ± 10 nm for NF1 to 1000 ± 300 for NF4.

To investigate whether electrospinning of fibers from TFA:acetone solution yield the piezoelectric δ'-phase of nylon-11, X-ray diffraction (XRD) have been performed. As the first step, two reference XRD measurements are performed on melt-quenched-stretched film (δ'-phase), and the drop-casted film from TFA solution (γ-phase), Figure S8, Supporting Information. For the melt-quenched and subsequently stretched (MQS) film, the diffraction peak is the sum of (100) and (010/110) reflections, which occur at an identical $2\theta = 20.95°$ and are referred as the interchain distance along the hydrogen bonds and the intersheet distance between the hydrogen-bonded sheets, respectively. The δ'-phase shows the largest lateral spacing of 0.424 nm between the sheets, which is also responsible for ferroelectricity in MQS samples of nylon-11.[30] For the γ-phase reference film, however, there are two clearly distinct peaks of (100) and (010/110) reflections, which are positioned at $2\theta = 21°$ and 21.3°, respectively. The d-spacings are given in **Table 1**, Supporting Information. The peak positions of the reference samples are taken as cue for the analysis of the nanofibers.

Table 1. d-spacing calculated from XRD patterns for different samples.

Diffraction peaks	d-spacing [nm]					
	δ'-phase film	γ-phase film	NF1	NF2	NF3	NF4
(001)	1.31	1.49	1.29	1.26	1.40	1.49
(100)	0.424	0.423	0.416	0.415	0.420	0.413
(010/110)		0.418	0.380	0.375		0.410

The XRD diffractograms of the nanofibers are given in **Figure 2**. For the fibers with thinnest diameter, that is, NF1 and NF2, the XRD diffractograms show a large broad peak, with a tiny peak on the shoulder at $2\theta = 24°$. Appearance of a clear peak at 24° is due to the presence of the α'-phase. The corresponding d-spacing of (100) and (010/110) reflections, after deconvolution, amounts to 0.415 and 0.375 nm, respectively, matching exactly with the reported peaks for the α'-phase.[30,31] Formation of the α'-phase is due to the better order of the molecular chains at small fiber diameters. The low viscosity of the nylon-11 solution combined with large potential gradient, force the nylon-11 chains to pack in a highly ordered structure. We note that all the diffraction peaks for the nanofibers appear narrower than those of the MQS films indicating better alignment of the polymer chains along the fiber direction. As the diameter of the nanofiber increases to 200 nm, NF3, the deconvoluted (100) and (010/110) reflections, hold exactly the same position as those shown in the reference MQS film of Figure S8a, Supporting Information. The NF3 fiber is therefore mainly composed of the δ'-phase crystalline structure. The (001) d-spacing amounts to 1.40 nm, slightly larger than the MQS film, which is due to the higher extension of polymer chains during electrospinning. However, further increase in the fiber diameter to 1000 nm, NF4, the (100) and (010/110) reflections split apart with a d-spacing of 0.413 and 0.410 nm, which indicates crystallization of the NF4 fiber in the γ-phase. This is further confirmed by the (001) reflection with d-spacing of 1.49 nm, which matches exactly the one obtained for the reference γ-phase film.[12]

Solvent evaporation rate plays a crucial role in formation of the piezoelectric phase in nylon-11. To achieve the δ'-phase in thin-films, fast solvent evaporation is needed. For NF1, NF2, and NF3, due to the large surface to volume ratio of the

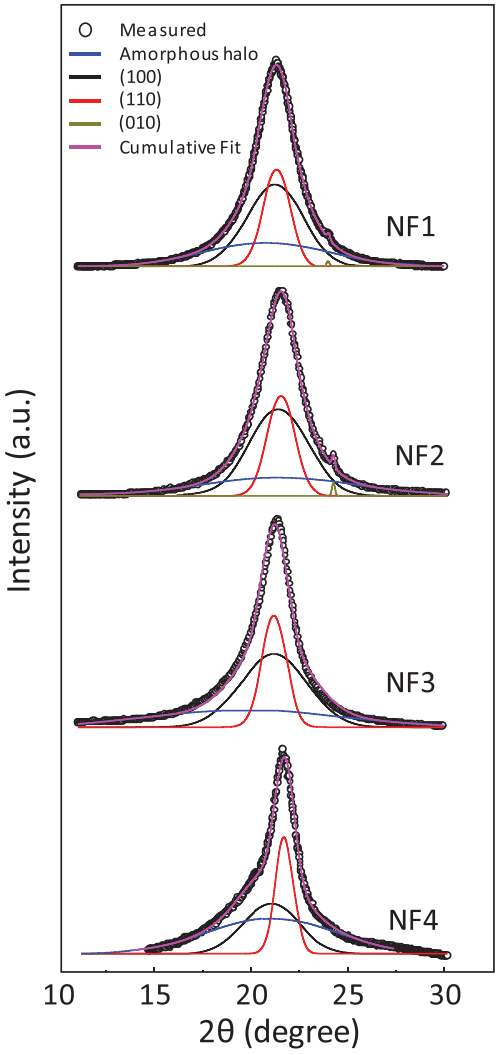

Figure 2. XRD diffraction of elctrospun nylon-11 fibers. The symbols show the measurement and the solid line show the deconvoluted peaks as well as the calculated XRD diffractograms.

nanofiber, the solvent evaporation rate is high. However, due to confinement of the NF1 and NF2 fibers to very small diameters, the mechanical stretching of the jet during the electrospinning induces highly ordered α'-phase. For the NF4 fibers, the diameter is large and the solvent evaporation rate is not fast enough and therefore γ-phase is formed. For the NF3 fiber, these conditions seem to be right and the solvent evaporation rate is fast enough to allow formation of majorly δ'-phase. Therefore, we speculate that the nylon-11 fibers, obtained by electrospinning from TFA:acetone solution with diameter range between 100 to 1000 nm, are majorly composed of δ'-phase.

Through controlling the processing condition, piezoelectric phase of nylon-11 can be readily achieved through electrospinning from TFA:acetone solution. The piezoelectric fiber can be therefore employed to harvest energy from mechanical vibrations. All the nanofibers generate voltage pulses upon impact, irrespective of the diameter. **Figure 3**a shows the generated voltage measured on the fiber mat under open circuit condition at the optimum external load, in response to a periodic mechanical impact with a frequency of 8 Hz. The amplitude of the voltage response strongly changes with the fiber diameter. The open circuit voltage for the thin NF1 and NF2 fibers is below 0.6 V, whereas for the NF3 fiber the voltage increases to 6 V, but then decreases again to 4 V for the thick NF4 fiber. The areal power output of the mats are experimentally determined by impedance matching with an external load, as shown in Figure 3b. All mats that are tested have similar thicknesses of nearly 50 µm, therefore volumetric power generated by the nanofibers follows the same trend albeit divided by thickness, which is a same division factor for all the nanofibers. We note that for the eventual application of the nanofibers the areal power density is a more relevant parameter.

The areal power output of the mats composed of NF1 and NF2 fiber is low with a maximum power of 0.03 µW cm^{-2} at 400 kΩ, whereas the NF3 and NF4 deliver an areal power output of 3.1 µW cm^{-2} (at 500 kΩ) and 2.6 µW cm^{-2} (at 800 kΩ), respectively. The trade-off between the fiber diameter and the generated voltage upon mechanical impact is directly related to the crystalline phases that are present in the fibers. Besides the crystallinity, the fiber diameter also affects the generated

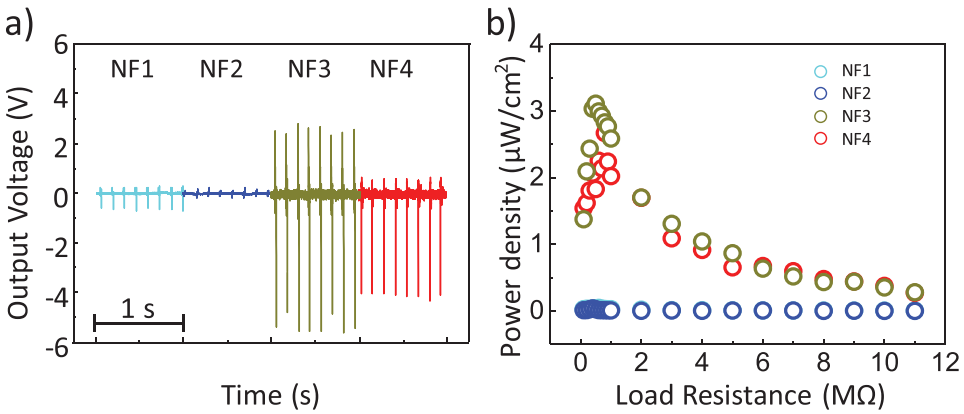

Figure 3. a) Open circuit output voltage of nylon-11 fibers with various diameters under mechanical impact. b) Power output as a function of load resistance for all nanofibers with various diameters.

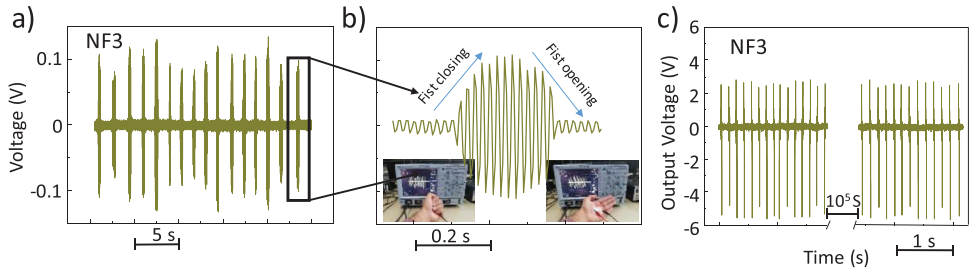

Figure 4. a) Real-time body motion monitoring: a piezoelectric nanogenerator is attached to palm which generates electrical signals upon closing and opening the fist. b) Zoom-in of (a). The inset shows the photographs of the fiber sensor attached to the hand and the output signals generated upon opening and closing of the fist. The signals are detected by an oscilloscope. c) Open circuit voltage of the NF3 nanofibers before and after continuous impacting for 10^5 s at a frequency of 8 Hz.

voltage. We will discuss the effect of diameter in the last section of the manuscript.

The NF3 fibers are very sensitive to mechanical excitations due to their crystallization in the electroactive δ'-phase, which makes them a potential candidate for detecting mechanical movement of body parts. To demonstrate the viability of the NF3 nanofibers for sensing applications, a nonwoven mat of NF3 fibers is placed on the hand, as shown in **Figure 4**b (inset). The nanofibers detect opening or closing of the fist through generating voltage pulses as shown in Figure 4a. As shown in Figure 4b, the output voltage increases and then drops upon closing and opening the fist, respectively. It should be noted that the profile of the voltages generated is directly related to the amount of force exerted on the nanofibers upon bending, which shows the sensitivity of the fibers to the external load. NF3 nanofibers are therefore capable to convert mechanical energy from human motions into electricity and enables the development of wearable nanogenerators based on nylon-11 fibers. It should be noted that although harvesting low frequency energy, particularly in the Hz regime is technically challenging, employing the recently developed plug-and-play energy harvesting circuits can further boost the output power of the nylon-11 fiber energy harvester.[32]

Durability of the nanofiber upon continuous mechanical impact is an important factor, which should be evaluated if nylon-11 fiber are considered for energy harvesting and sensing applications. Figure 4b shows the voltage generated by NF3 after experiencing mechanical impacts of 0.2 MPa, at an impact frequency of 8 Hz for 35 h. The fibers do not show any degradation in voltage output after 10^6 impacts, indicating durability of the NF3 fibers. Note that the largest electrical power available from human activity is from walking,[33] and 0.2 MPa is equivalent to the mean pressure between forefoot and heel of an average human while walking.[34] Now, assuming that the frequency of steps is around 1 Hz (one impact per second), and that a person walks on average 2 h per day, we would arrive at stable operation of at least 140 days.

At last, we have performed finite element method (FEM) calculations to I) elucidate the role of the diameter of nylon-11 fibers on the voltage response, II) investigate the sensitivity of the fibers toward mechanical deformations, and III) substantiate a proposal that substantially enhances the voltage generation capability of the nylon-11 (or alternatively improve their sensitivity to mechanical impacts). Details of the calculation, the mesh and the parameters are given in the supplementary information. The densities of α' and δ'-phases are taken as 1.17 and 1.04, respectively.[35] The contents for simulation of δ' and α'-phases are taken from literature.[16] A simplified nanofiber with variable diameter and fixed length of 500 nm is used, because the focus of the FEM simulation is to gain insight rather than reproducing the complex experimental situation (details of the simulation are given in Figure S10, Supporting Information). It is assumed that the nanofibers are self-poled and the polarization axis is along the diameter in the z-direction, and in parallel with the applied mechanical stress. In practice, the electrical outputs of nylon-11 nanofiber mats are generated from a complex network of such sections connected in series and parallel. First, we have considered two cases of thin and thick diameters of 55 and 200 nm, respectively, which corresponds to the cases for NF1 α'-phase and NF3 δ'-phase fibers. At first, both fibers experience the same cyclic mechanical impact of 0.25 MPa. The calculated peak voltages for both cases are presented in **Figure 5**a. The calculated peak voltage of the thin α'-phase fiber is only 3 mV, whereas the peak voltage output for the thicker δ'-phase fiber is four times larger and amounts to 12 mV. The calculation shows a factor of 4 increase in peak voltage of the nanofibers with an increase in fiber diameter from 55 to 200 nm. Experimentally, the peak voltage of NF3 is 6 V, which is about ten times larger than NF1 (≈0.6 V). Therefore, there is reasonable agreement between the simulation and experiment, considering the simplified model. Hence, the difference in the generated voltages by the different nanofibers can be primarily ascribed to the crystalline phase of nylon-11 in which the fiber is crystallized.

The δ'-phase nylon-11 fiber is very sensitive to the applied pressure, as shown in Figure 5b, where the generated peak voltage is calculated for the fibers under variable pressure. While both fibers show increase in the peak voltage, the δ'-phase fiber shows a much steeper increase in peak voltage. From the slope of the curves we obtained theoretical sensitivity of 0.13 mV kPa^{-1} for the δ'-phase fiber whereas the α'-phase fibers has only 0.02 mV kPa^{-1}.

The FEM simulation with a relatively good accuracy captures the physics behind the superior performance of δ'-phase NF3 fiber in energy harvesting and sensing. Hence, the model can be employed to evaluate different proposals to enhance the peak voltage of the δ'-phase nylon-11 fiber. It has been shown that energy harvesters based on porous P(VDF-TrFE) films as well as nanofibers, with pores that are confined inside the polymer, show enhanced power output of the

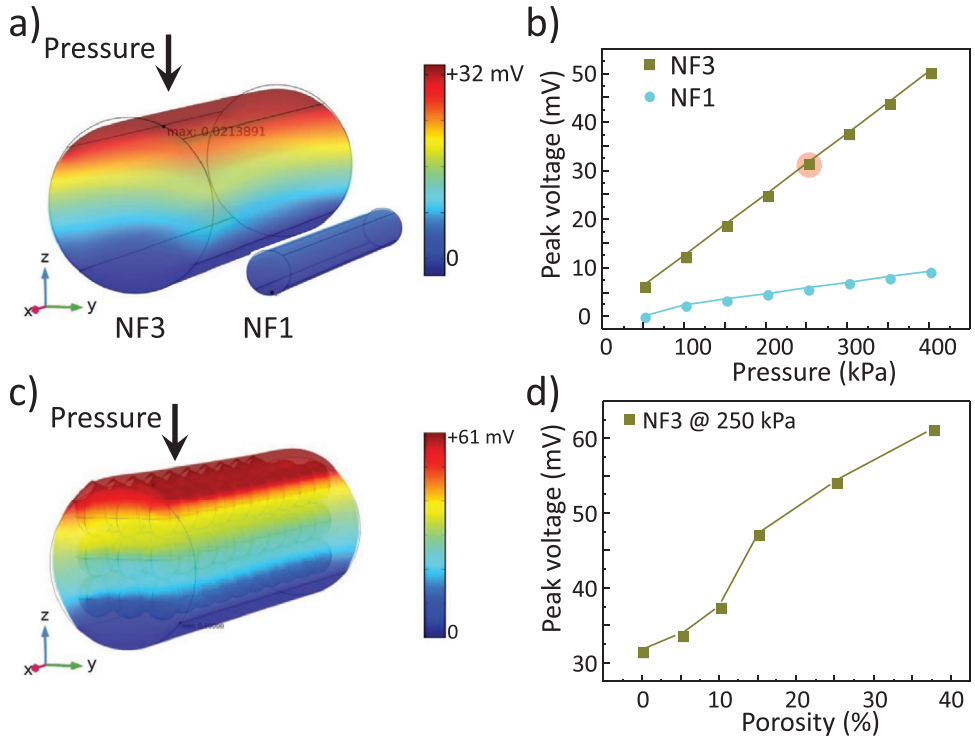

Figure 5. a) The graphic of the FEM simulation of the δ'-phase NF3 and α'-phase NF1 fibers under cyclic pressure of 250 kPa. b) The calculated voltage form the same fibers as a function of the applied pressure. c) The graphical simulation of the voltage peak for the δ'-phase NF3 fiber at a porosity of 37.5% under applied pressure of 250 kPa. d) The calculated peak voltage as function of porosity under applied pressure of 250 kPa.

generator.[36] In the next step of FEM simulations we therefore introduced spherical air cavities inside the δ'-phase nanofiber. The peak voltage is calculated for a fixed pressure of 250 kPa for stress-charge mode. Figure 5c shows a graphical profile of the generated voltage in the fiber with 37.5% porosity. The calculated peak voltage as a function of porosity is plotted in Figure 5d. The solid-core δ'-phase nanofiber produces a peak voltage of 32 mV. The peak voltage monotonically increases as the porosity enhances and reaches values as high as 61 mV. The enhancement of the peak voltage is due to lowering of the relative permittivity and the enhancing deformability of the nanofibers upon increasing the amounts of pores. For a porous dielectric film consisting of spherical closed pores, the relative permittivity, ε', decreases monotonically with the fractional porosity, P, as[36,37] $\varepsilon' = \varepsilon\left(1 - \frac{3P(\varepsilon-1)}{P\varepsilon + 1 - P + 2\varepsilon}\right)$, where, $\varepsilon = 4$[22] is the relative dielectric permittivity of nylon-11. For the ideal case of uniformly distributed isolated spherical pores, the dielectric permittivity continuously drops as porosity increases to 2.67 for a fiber that is 37.5% porous. Moreover, porosity substantially modifies the stiffness, specifically the elastic compressibility constant σ_{33} of the δ'-phase nylon-11 nanofibers. Both of these contributions are responsible for the enhanced peak voltage in the proposed porous nanofibers. Experimentally, various methods have been successfully exploited for the fabrication of porous nanofibers of non-piezoelectric nylons, which renders porous nylon-11 fiber a very promising candidate for the realization of highly efficient energy harvesters or sensitive pressure sensors.[38–40]

3. Conclusions

Piezoelectric nylon-11 nanofibers are produced by electrospinning from nylon-11 solution in TFA:acetone. The diameter of the nanofibers plays a crucial role in order to achieve the self-poled highly piezoelectric δ'-crystalline phase. It is postulated that formation of the δ'-phase is due to the interplay between the solvent mixture used for electrospinning, TFA:acetone, the solvent evaporation rate and the pulling force acting on the fiber during the electrospinning process. The electrical activity of the resulting nanofibers is maximum for the fibers that are crystalized in δ'-phase that produce a voltage as high as 6 V under mechanical impact, rendering the nylon-11 fibers a very promising candidate for wearable electricity generators. Moreover, the great sensitivity of the δ'-phase nylon-11 fibers to pressure can be exploited in sensing applications. It is substantiated through finite element modeling that introducing porosity inside the fibers is a viable route to enhance the voltage output. The demonstration of piezoelectric nylon fibers and concomitant guidelines for output power optimization opens a new route toward realization of smart and electronic textiles based on nylons.

4. Experimental Section

Materials: Nylon-11 was purchased from Sigma Aldrich. TFA and acetone (99.8%, Extra Dry), were purchased from Carl Roth Gmbh and ACROS Organics, respectively.

Table 2. Processing parameters for electrospinning and the resultant diameter of the fibers.

Sample	Solution concentration [wt%]	Applied voltage [kV]	Distance between spinneret and collector [cm]	Feed rate [mL h^{-1}]	Mean fiber diameter [nm]
NF1	5	15	15	0.05	55 ± 10
NF2	10	15	15	0.05	100 ± 20
NF3	15	15	15	0.1	200 ± 30
NF4	20	15	15	0.1	1000 ± 300

Solution Preparation and Electrospinning: First, the pellets of nylon-11 were dried in vacuum oven at 40 °C for 48 h. Nylon-11 solutions (different concentration: 5, 10, 15, and 20 wt%) were prepared by dissolving polymer in TFA and acetone mixture (60:40 mol%). The electrospinning process was carried out using a setup fabricated by IME Technologies with an applied voltage of 15–25 kV, a working distance between the spinneret and the collector of 15–25 cm, and a feeding rate ranging from 0.0025 to 1.0 mL h^{-1} as shown in **Table 2**. Nanofibers were collected on aluminum foils. The schematic of the electrospinning set up is given in Figure S3, Supporting Information.

As comparison, MQS films were prepared by hot pressing nylon-11 pellets at 210 °C for 2 min and immediately quenching in dryice–isopropanol solution. The films were uniaxially stretched at room temperature with a draw ratio of 3:1 at strain rate of 5 mm min^{-1} using a universal testing machine (Zwick Roell-Z005). The Υ-phase of the nylon-11 film was obtained by slow evaporation of the solvent at room temperature after drop casting the nylon-11 solution in TFA in a petri dish.

Microstructure Investigation: The diameter and morphology of nanofibers were examined with a Gemini 1530 (Carl Zeiss AG, Oberkochen, Germany) SEM, operating at an accelerating voltage of 0.35 kV. The nanofiber samples for SEM were prepared by depositing electrospun nanofibers directly on silicon wafers for about 5 s during electrospinning. The crystalline structures of the fibers and MQS film were investigated using an XRD (Philips Powder Diffractometer PW1820) using Cu radiation (l = 1.5418 Å).

Mechanical Impact Setup: The open circuit voltage was measured by an oscilloscope (LeCroy waverunner LT372) with an input resistance of 1 MΩ. The nanogenerators were subjected to periodic mechanical impacts at 8 Hz at an impact pressure of 0.2 MPa using a home-built set-up.

Fiber Sensor: A mat of fibers was placed on to a human hand for real-time motion detection. The motions of hand, by closing and opening of the fist, were recorded by oscilloscope. As nylons were inert and non-hazardous materials, they were widely used in wearable textiles, hence had the potential to be used as non-invasive health monitoring sensors. Informed, written consent from the participant in the test was obtained prior to the experiment.

Supporting Information

Supporting Information is available from the Wiley Online Library or from the author.

Acknowledgements

S.A. M.H.A, M.M.A, and K.A. acknowledge the financial support of the Alexander von Humboldt Foundation (Germany) through the Sofja Kovalevskaja Award, and the technical support from the Max-Planck Institute for Polymer Research. S.A. thanks the National University of Science and Technology (Pakistan) for the financial support. The authors wish to thank Prof. Paul. W. M. Blom for fruitful discussions and Dr. Manfred Wagner for the NMR measurement.

Open access funding enabled and organized by Projekt DEAL.

Conflict of Interest

The authors declare no conflict of interest.

Keywords

energy harvesting, nylon fibers, piezoelectric devices, sensors, smart textiles

Received: May 19, 2020
Revised: August 16, 2020
Published online:

[1] B. Chu, X. Zhou, K. Ren, B. Neese, M. Lin, Q. Wang, F. Bauer, Q. Zhang, *Science* **2006**, *313*, 334.
[2] R. Yang, Y. Qin, L. Dai, Z. L. Wang, *Nat. Nanotechnol.* **2009**, *4*, 34.
[3] K. Cherenack, L. van Pieterson, *J. Appl. Phys.* **2012**, *112*, 091301.
[4] S. Chalasani, J. M. Conrad, in *IEEE SoutheastCon 2008*, IEEE, Piscataway, NJ **2008**, pp. 442–447.
[5] D. V. Bayramol, N. Soin, T. Shah, E. Siores, D. Matsouka, S. Vassiliadis, in *Smart Textiles* (Eds: S. Schneegass, O. Amft), Springer, Cham **2017**, pp. 199–231.
[6] S. Park, Y. Kwon, M. Sung, B.-S. Lee, J. Bae, W.-R. Yu, *Mater. Des.* **2019**, *179*, 107889.
[7] J. Ning, M. Yang, H. Yang, Z. Xu, *Mater. Des.* **2016**, *109*, 264.
[8] L. Persano, C. Dagdeviren, Y. Su, Y. Zhang, S. Girardo, D. Pisignano, Y. Huang, J. A. Rogers, *Nat. Commun.* **2013**, *4*, 1633.
[9] S. Schellenberger, P. J. Hill, O. Levenstam, P. Gillgard, I. T. Cousins, M. Taylor, R. S. Blackburn, *J. Cleaner Prod.* **2019**, *217*, 134.
[10] P. Latko, D. Kolbuk, R. Kozera, A. Boczkowska, *J. Mater. Eng. Perform.* **2016**, *25*, 68.
[11] P. von Tiedemann, S. Anwar, U. Kemmer-Jonas, K. Asadi, H. Frey, *Macromol. Chem. Phys.* **2020**, *221*, 1900468.
[12] S. S. Nair, C. Ramesh, K. Tashiro, *Macromolecules* **2006**, *39*, 2841.
[13] Y. Shi, J. L. White, *Int. Polym. Process.* **1990**, *5*, 25.
[14] E. Balizer, J. Fedderly, D. Haught, B. Dickens, A. S. DeReggi, in *Conf. on Electrical Insulation and Dielectric Phenomena*, IEEE, Piscataway, NJ **1991**, pp. 193–200.
[15] J. Lee, Y. Takase, B. A. Newman, J. I. Scheinbeim, *J. Polym. Sci., Part B: Polym. Phys.* **1991**, *29*, 273.
[16] J. Lee, Y. Takase, B. A. Newman, J. I. Scheinbeim, *J. Polym. Sci., Part B: Polym. Phys.* **1991**, *29*, 279.
[17] Y. Takase, J. Lee, J. Scheinbeim, B. Newman, *Macromolecules* **1991**, *24*, 6644.
[18] J. Scheinbeim, J. Lee, B. Newman, *Macromolecules* **1992**, *25*, 3729.
[19] B. Mei, J. Scheinbeim, B. Newman, *Ferroelectrics* **1993**, *144*, 51.
[20] E. Balizer, J. Fedderly, D. Haught, B. Dickens, A. S. Dereggi, *J. Polym. Sci., Part B: Polym. Phys.* **1994**, *32*, 365.
[21] S. Ikeda, T. Saito, M. Nonomura, T. Koda, *Ferroelectrics* **1995**, *171*, 329.
[22] S. Anwar, B. Jeong, M. M. Abolhasani, W. Zajaczkowski, M. Hassanpour Amiri, K. Asadi, *J. Mater. Chem. C* **2020**, *8*, 5535.
[23] H. S. Nalwa, *Ferroelectric Polymers: Chemistry: Physics, and Applications*, CRC Press, Boca Raton, FL **1995**.
[24] I. Katsouras, K. Asadi, M. Li, T. B. Van Driel, K. S. Kjaer, D. Zhao, T. Lenz, Y. Gu, P. W. Blom, D. Damjanovic, *Nat. Mater.* **2016**, *15*, 78.

[25] H. H. Yu, *Mater. Chem. Phys.* **1998**, *56*, 289.
[26] A. Datta, Y. S. Choi, E. Chalmers, C. Ou, S. Kar-Narayan, *Adv. Funct. Mater.* **2017**, *27*, 1604262.
[27] D. Morais, R. Guedes, M. Lopes, *Materials* **2016**, *9*, 498.
[28] L. Chocinski-Arnault, V. Gaudefroy, J. L. Gacougnolle, A. Rivière, *J. Macromol. Sci. B* **2002**, *41*, 777.
[29] R. E. Lundin, F. E. Harris, L. K. Nash, *J. Am. Chem. Soc.* **1952**, *74*, 4654.
[30] J. W. Lee, Y. Takase, B. A. Newman, J. I. Scheinbeim, *J. Polym. Sci., Part B: Polym. Phys.* **1991**, *29*, 279.
[31] Z. Zhang, M. H. Litt, L. Zhu, *Macromolecules* **2016**, *49*, 3070.
[32] X. Wang, P. R. Wilson, R. B. Leite, G. Chen, H. Freitas, K. Asadi, E. C. P. Smits, I. Katsouras, P. R. F. Rocha, *Energy Technol.* **2020**, *8*, 2000114.
[33] J. L. Gonzalez, A. Rubio, F. Moll, *Int. J. Soc. Mater. Eng. Res.* **2002**, *10*, 34.
[34] D. Rosenbaum, S. Hautmann, M. Gold, L. Claes, *Gait Posture* **1994**, *2*, 191.
[35] S. M. Aharoni, *N-Nylons: Their Synthesis, Structure, and Properties*, Wiley, New York **1997**.
[36] M. M. Abolhasani, M. Naebe, K. Shirvanimoghaddam, H. Fashandi, H. Khayyam, M. Joordens, A. Pipertzis, S. Anwar, R. Berger, G. Floudas, J. Michels, K. Asadi, *Nano Energy* **2019**, *62*, 594.
[37] R. Richert, *Eur. Phys. J.: Spec. Top.* **2010**, *189*, 37.
[38] A. Gupta, C. D. Saquing, M. Afshari, A. E. Tonelli, S. A. Khan, R. Kotek, *Macromolecules* **2009**, *42*, 709.
[39] H. Zhang, L. Zhang, Q. Jia, C. Shi, J. Yang, *Polym. Eng. Sci.* **2015**, *55*, 1133.
[40] M. W. Frey, L. Li, *J. Eng. Fibers Fabr.* **2007**, *2*, 31.